NIH Public Access
Author Manuscript
Integr Biol (Camb). Author manuscript; available in PMC 2012 July 02.

Published in final edited form as:
Integr Biol (Camb). 2012 January ; 4(1): 10–21. doi:10.1039/c1ib00041a.

Single-molecule studies of nucleocytoplasmic transport: from one dimension to three dimensions

Alexander Goryaynov, **Jiong Ma**, and **Weidong Yang**
Department of Biological Sciences, Center for Photochemical Sciences, Bowling Green State University, Bowling Green, OH 43403, USA. wyang@bgsu.edu; Fax: +1 419-372-2024; Tel: +1 419-372-8007

Abstract

In eukaryotic cells, the bidirectional trafficking of proteins and genetic materials across the double-membrane nuclear envelope is mediated by nuclear pore complexes (NPCs). A highly selective barrier formed by the phenylalanine–glycine (FG)-nucleoporin (Nup) in the NPC allows for two transport modes: passive diffusion and transport receptor-facilitated translocation. Strict regulation of nucleocytoplasmic transport is crucial for cell survival, differentiation, growth and other essential activities. However, due to the limited knowledge of the native configuration of the FG-Nup barrier and the interactions between the transiting molecules and the barrier in the NPC, the precise nucleocytoplasmic transport mechanism remains unresolved. To refine the transport mechanism, single-molecule fluorescence microscopy methods have been employed to obtain the transport kinetics of individual fluorescent molecules through the NPC and to map the interactions between transiting molecules and the FG-Nup barrier. Important characteristics of nucleocytoplasmic transport, such as transport time, transport efficiency and spatial distribution of single transiting molecules in the NPC, have been obtained that could not be measured by either ensemble average methods or conventional electron microscopy. In this *critical review*, we discuss the development of various single-molecule techniques and their application to nucleocytoplasmic transport *in vitro* and *in vivo*. In particular, we highlight a recent advance from one-dimensional to three-dimensional single-molecule characterization of transport through the NPC and present a comprehensive understanding of the nucleocytoplasmic transport mechanism obtained by this new technical development (105 references).

Introduction

The nuclear pore complexes (NPCs) that are embedded in the nuclear envelope (NE) serve as a selective gate to mediate the exchange of macromolecules between the cytoplasm and the nucleus in eukaryotic cells. All gene-regulating proteins, nucleic acid polymerases, histones and splicing and transcription factors are imported to the nucleus after synthesis in the cytoplasm, and mRNAs and ribosomal subunits are exported to the cytoplasm after transcription in the nucleus.[1] Electron microscopy has revealed that the NPC is one of the largest molecular machines in the eukaryotic cell (Fig. 1).[2-14,92] In the NPC, the central framework encircles the central pore, which is ~40–90 nm in length and has a minimum internal diameter of ~40–75 nm.[2,3,5,13] On the cytoplasmic side, the cytoplasmic ring moiety caps the framework with eight short cytoplasmic filaments protruding into the cytoplasm by ~30–50 nm.[2,5,14] On the nuclear side of the NPC, the central framework is capped by a nuclear ring moiety connected to a distal ring by an assembly of eight filaments, forming a nuclear basket extending ~50–75 nm into the nucleoplasm from the inner nuclear membrane.[2-14]

The NPC is a large assembly composed of approximately 30 different proteins, known as nucleoporins (Nups), with each present in an integer multiple of eight copies.[1,15-20]

NIH-PA Author Manuscript
NIH-PA Author Manuscript
NIH-PA Author Manuscript

NIH-PA Author Manuscript

NIH-PA Author Manuscript

NIH-PA Author Manuscript

Approximately one-third of the total Nups possess a 'natively unfolded' structure, with domains that are rich in phenylalanine–glycine (FG) repeats.[1,15,16,21,22] These FG-Nups form the selective permeability barrier in the NPC that permits two transport modes: the passive diffusion of small molecules (<20–60 kDa) and the facilitated translocation of cargo molecules which have specific signals.[20,36,52-58,83,93] The passive diffusion of small molecules suggests that small molecules diffuse freely through the NPC without the consumption of chemical energy. By contrast, signal-dependent cargos must include specific targeting signals: nuclear localization signals (NLS) for nuclear import or nuclear export signals (NES) for nuclear export. These cargos can then be specifically recognized by soluble accessory proteins (importins/exportins), which mediate the transport of cargo complexes by transient interactions with the FG repeats in the NPC.[13,23-27] Importin β (Imp β)-type transport receptors account for the majority of the nuclear transport pathways.[28] They circulate between the nucleus and the cytoplasm, recognize cargo molecules and transfer them from one side of the NE to the other.[29] Substrate loading to and release from the Imp β-type transport receptors are regulated by a concentration gradient of RanGTP or RanGDP across the NE.[30-37,49,51] Multiple studies have shown that a series of rapid and low-affinity binding events between the transport receptors and the FG repeats along the NPC enhance efficient transport of receptor-cargo complexes through the NPC.[21,38-47] RanGTP is only hydrolyzed when the cargo complexes dissociate from the cytoplasmic side of the NPC after facilitated diffusion through the NPC.[30-37,49,51]

To understand the mechanism of nucleocytoplasmic transport, the transport kinetics and the pathways of either passive diffusion or facilitated translocation through the NPC under real-time trafficking conditions need to be measured. To achieve this, single-molecule fluorescence approaches have recently been developed to study nucleocytoplasmic transport.[48-58,94] In this paper, we will first review the peculiarities of FG-Nups and the promotion of facilitated translocation by the interactions between the FG-repeats and transport receptors that are predicted by various nucleocytoplasmic transport models. Second, we will review the recent application of single-molecule fluorescence methods to the study of nucleocytoplasmic transport by one-dimensional (1D) localization of molecules transiting around the NE. Finally, we will highlight a technical development from 1D to 3D determination of the spatial location distribution of single transiting molecules within single NPCs and present a comprehensive understanding of the nucleocytoplasmic transport mechanism revealed by this latest technical advance.

Interactions between the FG-Nups and transport receptors

The Nups anchored in the NPC approximately form three discrete layers depending on their spatial locations in the NPC.[59-60] The Nups with α-solenoid and β-propeller folds anchor the NPC in the NE and form the "scaffold layer" in the NPC central framework. The Nups on the peripheral side of the NPC are comprised of α-helices and cadherin folds and generate the "membrane layer". The last but not the least important group of Nups, which have domains rich in FG repeats, forms the "inner layer" on the inner surface of the NPC. These Nups exhibit structural characteristics typical for "natively unfolded" and "intrinsically disordered" proteins.[1,60,61,95,96] These FG-Nups provide about 2700 FG-repeats along the NPC; the FG motifs include FG, FXFG (Phe-any-Phe-Gly) or GLFG (Gly-Leu-Phe-Gly).[3,62] The FG-Nups with different FG types are distributed along the NPC in vertebrates. Two Nups that predominantly contain FXFG (Nup 153 and Nup 50) are found on the nuclear-basket side of the NPC. Four FG-repeat-containing Nups (POM 121, Nup 54, Nup 58 and Nup 45), one FXFG-Nup (Nup 62) and one GLFG-Nup (Nup 98) are distributed centrally or symmetrically around the scaffold of the NPC. On the cytoplasmicfibrils side, there are two FG-Nups (Nup 214 and hCG1) and a single FXFG-Nup (Nup 358).[62]

NIH-PA Author Manuscript

NIH-PA Author Manuscript

NIH-PA Author Manuscript

The FG-family of Nups is the main component of the selective gate of the NPC and is critical for the process of nucleocytoplasmic transport.[63] Although the mechanism of facilitated translocation through the NPC is not fully understood, interactions between the transport receptors and the FG-Nups are apparently central to the process. Numerous models have been proposed to explain how these interactions promote the efficient translocation of cargo complexes through the NPC. The "virtual gating" model suggests that the NPCs act as an entropic barrier and increase the activation energy that is required for a molecule to enter the narrow nuclear pore for the translocation process. The activation energy can be reduced by transport receptors through binding to the FG repeats.[64] Previous *in vitro* data revealed that 33 nM Imp β1 collapses the FG-filaments of Nup153 toward their anchoring sites and that the addition of RanGTP can reverse the collapse.[45] Based on this experimental observation, the "polymer brush" model suggests that the FG-filaments in the NPC can form extended polymer brushes that grant access to large molecules only if they interact with the filaments. To allow the transport complexes to enter the pore, the FG-filaments collapse in the presence of transport receptors.[45] Additionally, the "oil spaghetti" model proposes that the long hydrophobic FG repeats shroud the NPC channel. The oil-spaghetti-like FG filaments can be pushed aside by transport receptor-cargo complexes.[19] Furthermore, in the "reduction dimensionality model (ROD)", the FG-filaments would be permanently collapsed by transport receptors with a saturated concentration in the NPC.[12,65] The collapsed FG-filaments would form a coherent FG-receptor bilayer at the inner surface of the nuclear pore and leave an open axial central tube through the NPC. Small molecules could passively diffuse through the central tube and transport receptors or receptor-cargo complexes could diffuse two-dimensionally along the FG-repeats-coated wall.[12,65]

In contrast to the above models, the "selective phase/hydrogel" model speculates that the NPC is a FG-Nup meshwork with gel-like properties that mechanically restricts access to larger molecules while allowing the free passage of small molecules.[20,66-68] The size of the FG mesh functions as a size restriction for large molecules and determines the upper limits of passive diffusion. Therefore, there are multiple channels (with diameters r 2.6 nm) for the passive diffusion of small molecules that are randomly distributed throughout the NPC.[97] Transport receptors are able to get through the barrier by transiently interacting with the FG-repeats and dissolving the FG-FG meshwork across the NPC. Clearly this model does not suggest the physical collapse of the FG-filaments towards their anchors in the NPC.

In addition, based on the latest analysis of the hydrodynamic properties of the FG-domains, the "forest" model suggests that the selective permeability barrier consists of the collapsed FG-Nups (called "shrubs") and the extended or relaxed FG-Nups (called "trees").[69,70] In this model, there are two separate zones for either passive diffusion of small molecules or facilitated translocation of cargo complexes. One zone would be a central axial tunnel in the NPC, and the other zone would be located at the periphery of the central tunnel.[70]

1D single-molecule characterization of nucleocytoplasmic transport

Over the years, ensemble measurements that report averaged outcomes have provided the basis for our understanding of the nucleocytoplasmic transport system. The use of ensemble measurements has identified various transport receptors and signaling pathways that enable efficient trafficking of different transport modes.[20,66-68,98] Ensemble methods have been and will continue to be one of the major investigatory approaches for eventually unraveling the mechanism of nuclear transport. However, important information is inevitably lost in the averaged outcome of ensemble experiments, such as the transient intermediate status of molecules, a minority of spatially or temporally localized signals, and non-synchronized events. For example, how many transient interaction sites are there between the transport receptors and the FG barrier in each NPC? What is the residence time and spatial location of each interaction during functional transport? Does the conformation of the FG barrier in the

NIH-PA Author Manuscript

NIH-PA Author Manuscript

NIH-PA Author Manuscript

NPC change under different nucleocytoplasmic trafficking conditions? There are many such questions, and the answers to these questions are extremely important for distinguishing between the current transport models and ultimately unraveling the nucleocytoplasmic transport mechanism. Clearly, assessing such detailed dynamic information is beyond the capabilities of population methods.

An entirely new field of science, often referred to as single-molecule biology, has emerged and developed rapidly in recent years. Single-molecule methods provide a truly innovative approach to investigating biological/biochemical/biomedical problems by distinguishing, monitoring, tracking and controlling individual bio-molecules *in vitro* and *in vivo*. There are three main categories of single-molecule methods: mechanical, electrical and optical approaches. Given its inherently noninvasive method of detection, fluorescence microscopy imaging has emerged as the most appropriate method for observing specific components or processes in living cells, tissues, and whole organisms. However, owing to diffraction, a wave of light cannot be focused to an arbitrarily small point. Conventional fluorescence microscopes therefore have long been thought to be incapable of resolving two objects that are closer together than approximately half the wavelength of the light, with an imaging resolution of approximately 200 nm laterally and 600 nm axially. Recently, a number of fluorescence imaging techniques have pushed the boundaries of optical resolution below the diffraction limit, as low as several nanometres.[71-78,99,100] The fundamental principle is that the position of an isolated fluorescent emitter can be precisely determined by finding the centroid of its image, although its image appears as a diffraction-limited spot. The precision of this localization process is determined by the ratio of the total number of photons collected from the single emitter to the background noise. This concept has been used to track spatial locations of fluorescent particles with nanometre-scale accuracy. Recently it has been shown that, even when the emitter is a single fluorescent dye molecule attached to a motor protein, the position of the emitter can be determined with a precision as high as 1–3 nm with a 500 ms exposure time *in vitro*.[75,76,101,102,79]

Undoubtedly, imaging and tracking individual transiting molecules through single NPCs will be essential for measuring detailed transport kinetics and spatial information in the NPC. To pursue this goal, deep penetration into the cell, fast imaging of single transiting molecules interacting with the NPC and localization of these single molecules with high spatial resolution are required for the selected single-molecule method. In the past, epifluorescence microscopy has been widely used as one of the primary tools for elucidating the interaction time, the transport efficiency of individual transiting molecules through the NE and the relative spatial locations of the transiting molecules from the middle plane of the NE in permeabilized and live cells.[52,54,55,80,81] Conventional wide-field epifluorescence microscopy[82] has been used to illuminate the entire NE and image single-molecule transport events through the NE (Fig. 2A). However, this technique suffers from a low signal-to-noise (S/N) ratio for single-molecule tracking due to significant noise from the background fluorescence emitted from out-of-focal-plane fluorescent molecules. To gain a higher S/N ratio, narrow-field epifluorescence microscopy was developed by introducing a micrometre-sized pinhole to confine the excitation light beam.[54,55,83] A narrower excitation beam generates a smaller excitation volume in and out of the focal plane and greatly reduces the noise from background fluorescence (Fig. 2A). Such a modification can generate an approximately two-fold improvement in the S/N ratio, and the improved S/N ratio can enhance the spatial localization of single fluorescent molecules.[83] The wide-field epifluorescence method has a spatial resolution of approximately 30 nm at 5 ms;[48-53] by contrast, the narrow-field method has a spatial resolution of approximately 15 nm at 2 ms.[54,55,83] The higher spatiotemporal resolution results in a more accurate determination of the transport kinetics on the NE.

NIH-PA Author Manuscript

NIH-PA Author Manuscript

NIH-PA Author Manuscript

To characterize nucleocytoplasmic transport at the single-molecule level by either wide-field or narrow-field epifluorescence microscopy, the localization of the NE at the equator of the nucleus first needs to be determined. Two different methods have been used to localize the middle plane of the NE: one uses the bright-field image of the NE obtained from the contrast between the NE and the compartments on either side, while the other obtains fluorescent images of the NE by conjugating green fluorescence protein (GFP) or other fluorescent proteins to at least one Nup anchored in the NPC.[50,52,55,58] To distinguish individual NPCs on the NE, the fluorescent method is preferred. By either wide-field or narrow-field epifluorescence microscopy, fluorescent imaging of the NE has shown that the individual NPCs embedded on the NE cannot be distinguished well due to the short distances between the neighboring NPCs,[58] which results in a heavily overlapped GFP-NPC fluorescence, as shown in Fig. 2B. But, the middle plane of the NE can be obtained with certainty by Gaussian fitting of the line-scanned pixel intensity in the *x* dimension, as shown in Fig. 2B. Then, fluorescent transiting molecules can be added into the cytoplasm or nucleus of the cell at nanomolar levels, and the spatial locations of the individual molecules within each detection frame can be subsequently determined by 2D Gaussian fitting of the centroid of each single-molecule fluorescent spot. As an example, a functional individual molecule was added into the cytoplasm of a permeabilized cell under recombined transport conditions.[54,55,58,83] Starting in the cytoplasm, the molecule was observed to approach the NE, interact with the NE and arrive in the nucleus (Fig. 2C–D). Because the NPC is the only portal for trafficking between the cytoplasm and nucleus, it was assumed that the observed molecules interacted with and traveled through the NPC. Thus, the interaction time between the transiting molecules and the NE (the spatial locations of single molecules fall into the 100 nm range around the middle plane of the NE) are counted as the dwell time of the transiting molecules in the NPC (Fig. 2D). Moreover, the dwell time consists of two components. If the transiting molecules successfully transverse the NE, this dwell time only represents the transport time for complete events. By contrast, if transiting molecules return to their original compartments after interacting with the NE, the dwell time suggests the transport time for abortive transport events. Approximately 50% of the molecules undergoing either passive or facilitated transport through the NE were found to successfully complete their transport.[55] Therefore, the transport efficiency, which is defined as the percentage of total transport events that are complete transport events, is 50%. Interestingly, the transport efficiency can be further regulated by the nuclear pore occupancy of Imp β1.[55]

In addition to the transport kinetics, the distribution of transiting molecules perpendicular to the tangent direction of the middle plane of the NE can also be obtained from the determination of the relative distances between the single-molecule locations and the middle plane of the NE. Hundreds or even thousands of such single-molecule trajectories were collected and superimposed, which generated a 1D spatial distribution of the transiting molecules around the NE, as shown in Fig. 2E. From the histogram of the spatial locations, the major interaction sites between the transiting molecules and the NPC could be drawn. However, the later 2D and 3D spatial maps of the interaction sites inside the NPC revealed that there was much more information hidden from the 1D characterization.[58] Besides, FCS algorithm was also used to monitor model proteins undergoing transport through the NE in living cells.[81,94]

Despite the above limitations, 1D characterizations of nucleocytoplasmic transport have provided a series of important transport kinetics through the NE *in vitro* and *in vivo*,[48-57,103-105] as summarized in Table 1. The major results include the following: (i) the transport time through the NPC is on the millisecond level for various-sized molecules, which is much faster than the previously estimated transport time; (ii) whatever the size of the functional cargo molecules studied, all of them perform a bidirectional, random diffusion through the NPC, and an approximate 50% transport efficiency is obtained for a series of

NIH-PA Author Manuscript

NIH-PA Author Manuscript

NIH-PA Author Manuscript

passive and facilitated transport; (iii) transiting molecules undergo continuous interactions with the NPC, and these interactions either concentrate at the central pore or mainly distribute on either side of the NPC. Overall, the aforementioned fluorescence microscopy methods can provide transport kinetics and 1D spatial information for molecules transiting through the NE with a spatiotemporal resolution of 15–30 nm and 1–3 ms. However, many critical questions remain unresolved by the current 1D single-molecule approach. (1) Do the observed interactions truly occur in the NPCs? (2) What is the spatial distribution of these interaction sites in the NPC? (3) Is there an open central channel for passive diffusion of small molecules, as proposed by various transport models? (4) Are the passive and facilitated transport processes common or separate pathways in the NPC? (5) Can the structure of the selectivity barrier formed by the unfolded FG-Nups in the NPC be measured? To answer these questions, we need to spatially localize single NPCs in live cells and further colocalize the trajectories of the transiting molecules with the determined individual NPCs to obtain 2D or even 3D transport information. In addition, a higher localization precision and a better temporal resolution are needed to maximally capture transient diffusion or interactions for various cargo molecules through the NPC.

3D single-molecule characterization of nucleocytoplasmic transport

To obtain precise spatial locations of transient interactions between the transiting molecules and the NPCs in a non-invasive fashion in three dimensions, 3D single-molecule tracking techniques with high spatiotemporal resolution are urgently needed. Many new single-molecule techniques with super-spatial resolution have been developed recently. Briefly, stimulated emission depletion (STED),[84] stochastic optical reconstruction microscopy (STORM),[85] photoactivated localization microscopy (PALM)[86] and fluorescence photoactivation localization microscopy (FPALM)[87] can be grouped as “super-resolution single-molecule localization” approaches.[88,89] When combined with *z*-scanning, these approaches can further provide a 3D super-resolution image by reconstruction from the mapped coordinates obtained by the massive parallel localization through wide-field imaging. These methods can achieve a lateral precision of up to 25 nm and an axial localization precision of up to 50 nm over a depth of several hundred nanometres to several micrometres in the *z*-axis.[90] However, the temporal resolution is inevitably sacrificed, to minutes or even hours, to obtain a high 3D spatial resolution. Such low temporal resolutions are far above the millisecond-level transport time for substrates moving through the NPC and hence cannot be directly employed to determine nucleocytoplasmic transport in three dimensions. Here we describe a novel technique, single-point edge-excitation sub-diffraction (SPEED) microscopy, which is capable of providing an unprecedented spatiotemporal resolution of 9 nm and 400 μs for the direct capture of 2D spatial locations in the NPCs; 3D spatial density maps of the transient interactions in the NPCs are subsequently acquired through a deconvolution algorithm.[58]

SPEED microscopy

In SPEED microcopy,[58] an inclined diffraction-limited spot illumination volume is formed in the focal plane by combining some features of laser confocal microscopy (LCM) and total internal reflection fluorescence (TIRF) microscopy (Fig. 3A). First, unlike LCM, the SPEED setup has no pinhole in the emission path, which allows the detector, a CCD camera, to receive more signals while preserving an acceptable background fluorescence. Second, the illumination volume in the axial direction is reduced by shifting the laser beam off the center of the objective to form an inclined illumination volume with a refraction angle of 451 in the focal plane, rather than a total reflection as in TIRF microscopy (Fig. 3B). With an inclined diffraction-limit spot, SPEED microscopy allows only a single GFP-NPC illuminated by a 488 nm laser beam in the focal plane. When fitted with a 2D elliptical Gaussian function, the centroid of the well-isolated GFP-NPC can be determined with a spatial localization

NIH-PA Author Manuscript

NIH-PA Author Manuscript

NIH-PA Author Manuscript

accuracy of approximately 1.3 nm by collecting more than a million photons from 8 copies of GFP in the NPC (Fig. 3C).

A second laser, a 633 nm laser beam that follows the same beam path as the 488 nm laser, is used to excite single Alexa Fluor 647-labeled molecules transiting through the illuminated NPC (Fig. 3A). To reduce the photobleaching effect on the fluorescent transiting molecules, the laser excitation is modulated by an optical chopper to have an on-off mode. Single-molecule imaging resolution improves with photon counts, which can be enhanced by using a longer detection time or brighter emitters. Using a several-hundred-millisecond detection time or several hundred dye-labeled cargo molecules, the spatial localization precision can be improved to several nanometres.[75,76,79] However, a sub-millisecond temporal resolution and functional fluorescent transiting molecules were needed for our experiments. Thus, neither a longer detection time nor heavily labeled transiting molecules could be used. Instead a solution was found by squeezing the maximum number of photons from a single lightly-labeled molecule within a sub-millisecond detection time by generating a very high optical density in the illumination volume. Finally, with a 400 μs detection time and an average optical density of 500 kW cm^{-2} in the illumination area, approximately 1100 photons were obtained from a single substrate molecule labeled with four molecules of Alexa Fluor 647 (Fig. 4). The corresponding localization precision was 9 ± 1 nm for the immobile fluorescent molecules and 10 ± nm for the moving molecules (Fig. 4B). Notably, the sub-millisecond ± detection time not only enabled the capture of more transient interacting/diffusion steps in the single NPC but also enhanced the spatial localization precision of single moving particles. As shown in Fig. 4C, with a 10 ms detection time, the localization precision is two-fold worse than that obtained with a detection time of 400 μs. In addition, the system error of alignment between the red and green fluorescence channels is approximately 3.0 nm, which was determined by measuring 230 immobile Alexa Fluor 647-labeled GFP fluorescent molecules on the surface of the coverslip. Therefore, the total localization precision for single transiting molecules through the NPC is about 10.6 nm.

With the obtained high spatiotemporal resolution, real-time transient transport events can be acquired within single fluorescent NPCs. For example, a typical import event of Imp β1 through a single NPC is shown in Fig. 5A. The spatial trajectories of Imp β1 were obtained within a relative distance from the centroid of the NPC in two dimensions (Fig. 5B). Once hundreds of transport events were collected and superimposed, their 2D trajectories clearly demonstrated the spatial distribution of Imp β1 in the NPC; they primarily concentrated in a region around the centroid of the NPC and obviously highlighted the void spaces at the location of the NE, as expected. Thus a 2D spatial location map for transiting molecules in the NPC was plotted (Fig. 5C), which provided more details of the spatial locations of the transiting molecules in the NPC than did the 1D characterization. The map suggests a uniform distribution of Imp β1 molecules in the NPC. The histogram evaluating the locations of these molecules further suggests their symmetrical distribution and intensive interactions on both sides of the NPC in the x dimension (Fig. 5D), while the histogram of the locations in the y dimension suggests that there could be multiple interaction sites and Imp β1 molecules could diffuse to any region at the cross-section of the NPC (Fig. 5E). However, once the corresponding 3D density map was obtained, it was revealed that the above results do not give the complete story and were even incorrect.[58]

From 2D spatial locations to a 3D density map

The previously acquired 2D spatial distribution in the xy plane was actually a projection of the corresponding actual 3D spatial movements in the NPC. Each location of a single molecule at the cross-section of an NPC was represented by a coordinate (r, θ) in a cylindrical coordinate system (r, θ, x), where x refers to the position along the NPC axis (Fig. 6A). A uniform distribution of spatial locations in the θ dimension was formed by

NIH-PA Author Manuscript

NIH-PA Author Manuscript

NIH-PA Author Manuscript

combining the single-molecule trajectories of multiple NPCs based on overlapping centroids but without a reference point in the θ dimension. This cylindrical coordinate system was further simplified as (r, x) due to a constant distribution of molecules in the θ dimension. Therefore, the coordinates (r, x) were definitively obtained from the Cartesian coordinates (x, y) by means of a deconvolution process. The deconvolution of the obtained histogram in the y dimension revealed that the spatial densities of the Imp β1 locations in the r dimension clustered into distinct groups in different regions (Fig. 6B-C). Using 3D modeling software, a structure corresponding to the 3D spatial density map in the NPC was generated (Fig. 6D). The detailed conversion matrix and equations were presented in our previous report.[58]

The 3D spatial density map of the interaction sites between Imp β1 and the NPC provided novel insights into nucleocytoplasmic transport that could not be obtained from a 1D or 2D characterization: (1) the actual pathway of the facilitated translocation through the NPC depends more on the spatial distribution of the FG Nups than on the NPC architecture; (2) the spatial density of the effective interaction sites between Imp β1 and the FG Nups gradually increases from both sides of the NPC and is highest in the central pore region; and (3) cargo-free or cargo-bound Imp β1 rarely occupies an axial channel with a diameter of approximately 10–20 nm at its narrowest point through the NPC. Using SPEED microscopy, small molecules were recently found to passively diffuse through this axial central channel, and therefore these molecules follow a pathway other than facilitated translocation through the NPC.[91] The 3D imaging approach clearly provides strong evidence to support the configuration of a single central channel in the NPC[91] and could be further applied to unravel the structure of the FG-barrier in the NPC.

Conclusion

To investigate and refine the mechanism of nucleocytoplasmic transport, new approaches with the ability to precisely visualize and locate transient interactions between transport receptors, large cargo complexes and the ill-defined FG-Nups in the NPC are urgently needed. In this review, we highlighted the development of single-molecule techniques and the applications of these methods to nucleocytoplasmic transport *in vitro* and *in vivo*. In particular, we highlighted a recent advance from one-dimensional to three-dimensional single-molecule characterization of nuclear transport through the native NPCs. With a high spatiotemporal resolution of 9 nm and 400 μs, the newly developed SPEED microscopic technique permits the creation of 3D spatial density maps of transient interactions of various transiting molecules in single NPCs. The 3D imaging results have provided unprecedented details of the transport kinetics and spatial information about the process of nucleocytoplasmic transport, which can be used to distinguish between the current transport models and further refine our understanding of the nucleocytoplasmic transport mechanism. The future application of this method may ultimately result in the creation of a tool that can finally establish the structure of the FG-barrier in the NPC through snapshots of the transient spatial distribution of the FG repeats in the native NPCs. This method could also potentially be applied to the measurement of fast kinetics in other sub-cellular cavities of live cells.

Acknowledgments

We thank the National Institutes of Health for grant support (GM094041 and GM097037) and apologize to those colleagues whose work was not discussed or cited in this review because of space considerations.

Abbreviations

NPC nuclear pore complex

NIH-PA Author Manuscript

NIH-PA Author Manuscript

NIH-PA Author Manuscript

Imp β1	importin β1
Nups	nucleoporins
FG	phenylalanine-glycine
SPEED	single-point edge-excitation sub-diffraction

References

1. Tran EJ, Wente SR. Cell. 2006; 125:1041–1053. [PubMed: 16777596]
2. Beck M, Forster F, Ecke M, Plitzko JM, Melchior F, Gerisch G, Baumeister W, Medalia O. Science. 2004; 306:1387–1390. [PubMed: 15514115]
3. Stoffler D, Feja B, Fahrenkrog B, Walz J, Typke D, Aebi U. J. Mol. Biol. 2003; 328:119–130. [PubMed: 12684002]
4. Akey CW, Radermacher M. J. Cell Biol. 1993; 122:1–19. [PubMed: 8314837]
5. Beck M, Lucic V, Forster F, Baumeister W, Medalia O. Nature. 2007; 449:611–615. [PubMed: 17851530]
6. Pante N, Kann M. Mol. Biol. Cell. 2002; 13:425–434. [PubMed: 11854401]
7. Fahrenkrog B, Hurt EC, Aebi U, Pante N. J. Cell Biol. 1998; 143:577–588. [PubMed: 9813081]
8. Yang Q, Rout MP, Akey CW. Mol. Cell. 1998; 1:223–234. [PubMed: 9659919]
9. Cohen M, Tzur YB, Neufeld E, Feinstein N, Delannoy MR, Wilson KL, Gruenbaum Y. J. Struct. Biol. 2002; 140:232–240. [PubMed: 12490171]
10. Kiseleva E, Allen TD, Rutherford S, Bucci M, Wente SR, Goldberg MW. J. Struct. Biol. 2004; 145:272–288. [PubMed: 14960378]
11. Rout MP, Blobel G. J. Cell Biol. 1993; 123:771–783. [PubMed: 8227139]
12. Peters R. BioEssays. 2009; 31:466–477. [PubMed: 19274657]
13. Lim R, Aebi U, Fahrenkrog B. Histochem. Cell Biol. 2008; 129:105–116. [PubMed: 18228033]
14. Fahrenkrog B, Aebi U. Nat. Rev. Mol. Cell Biol. 2003; 4:757–766. [PubMed: 14570049]
15. Cronshaw JM, Krutchinsky AN, Zhang W, Chait BT, Matunis MJ. J. Cell Biol. 2002; 158:915–927. [PubMed: 12196509]
16. Rout MP, Aitchison JD, Suprapto A, Hjertaas K, Zhao Y, Chait BT. J. Cell Biol. 2000; 148:635–652. [PubMed: 10684247]
17. Lim RYH, Fahrenkrog B. Curr. Opin. Cell Biol. 2006; 18:342–347. [PubMed: 16631361]
18. Ben-Efraim I, Gerace L. J. Cell Biol. 2001; 152:411–417. [PubMed: 11266456]
19. Macara IG. Microbiol. Mol. Biol. Rev. 2001; 65:570–594. [PubMed: 11729264]
20. Ribbeck K, Gorlich D. EMBO J. 2002; 21:2664–2671. [PubMed: 12032079]
21. Denning DP, Patel SS, Uversky V, Fink AL, Rexach M. Proc. Natl. Acad. Sci. U. S. A. 2003; 100:2450–2455. [PubMed: 12604785]
22. Strawn LA, Shen T, Shulga N, Goldfarb DS, Wente SR. Nat. Cell Biol. 2004; 6:197–206. [PubMed: 15039779]
23. Suntharalingam M, Wente SR. Dev. Cell. 2003; 4:775–789. [PubMed: 12791264]
24. Rexach M, Blobel G. Cell. 1995; 83:683–692. [PubMed: 8521485]
25. Wozniak RW, Rout MP, Aitchison JD. Trends Cell Biol. 1998; 8:184–188. [PubMed: 9695836]
26. Stewart M. Nat. Rev. Mol. Cell Biol. 2007; 8:195–208. [PubMed: 17287812]
27. Cook A, Bono F, Jinek M, Conti E. Annu. Rev. Biochem. 2007; 76:647–671. [PubMed: 17506639]
28. Bayliss R, Littlewood T, Stewart M. Cell. 2000; 102:99–108. [PubMed: 10929717]
29. Nakielny S, Dreyfuss G. Cell. 1999; 99:677–690. [PubMed: 10619422]
30. Lyman SK, Guan T, Bednenko J, Wodrich H, Gerace L. J. Cell Biol. 2002; 159:55–67. [PubMed: 12370244]
31. Moore MS, Blobel G. Nature. 1993; 365:661–663. [PubMed: 8413630]

NIH-PA Author Manuscript NIH-PA Author Manuscript NIH-PA Author Manuscript

32. Walther TC, Pickersgill HS, Cordes VC, Goldberg MW, Allen TD, Mattaj IW, Fornerod M. J. Cell Biol. 2002; 158:63–77. [PubMed: 12105182]
33. Coutavas E, Ren M, Oppenheim JD, D'Eustachio P, Rush MG. Nature. 1993; 366:585–587. [PubMed: 8255297]
34. Bischoff FR, Klebe C, Kretschmer J, Wittinghofer A, Ponstingl H. Proc. Natl. Acad. Sci. U. S. A. 1994; 91:2587–2591. [PubMed: 8146159]
35. Yokoyama N, Hayashi N, Seki T, Pante N, Ohba T, Nishii K, Kuma K, Hayashida T, Miyata T, Aebi U, Fukui M, Nishimoto T. Nature. 1995; 376:184–188. [PubMed: 7603572]
36. Bischoff FR, Görlich D. FEBS Lett. 1997; 419:249–254. [PubMed: 9428644]
37. Izaurralde E, Kutay U, von Kobbe C, Mattaj IW, Gorlich D. EMBO J. 1997; 16:6535–6547. [PubMed: 9351834]
38. Bednenko J, Cingolani G, Gerace L. J. Cell Biol. 2003; 162:391–401. [PubMed: 12885761]
39. Bischoff FR, Ponstingl H. Nature. 1991; 354:80–82. [PubMed: 1944575]
40. Chaillan-Huntington C, Butler PJ, Huntington JA, Akin D, Feldherr C, Stewart M. J. Mol. Biol. 2001; 314:465–477. [PubMed: 11846560]
41. Corbett AH, Silver PA. J. Biol. Chem. 1996; 271:18477–18484. [PubMed: 8702493]
42. Fried H, Kutay U. Cell. Mol. Life Sci. 2003; 60:1659–1688. [PubMed: 14504656]
43. Isgro TA, Schulten K. Structure. 2005; 13:1869–1879. [PubMed: 16338415]
44. Lee SJ, Matsuura Y, Liu SM, Stewart M. Nature. 2005; 435:693–696. [PubMed: 15864302]
45. Lim RYH, Fahrenkrog B, Koser J, Schwarz-Herion K, Deng J, Aebi U. Science. 2007; 318:640–643. [PubMed: 17916694]
46. Liu SM, Stewart M. J. Mol. Biol. 2005; 349:515–525. [PubMed: 15878174]
47. Paschal BM, Gerace L. J. Cell Biol. 1995; 129:925–937. [PubMed: 7744965]
48. Babcock HP, Chen C, Zhuang X. Biophys. J. 2004; 87:2749–2758. [PubMed: 15454466]
49. Dange T, Grünwald D, Grünwald A, Peters R, Kubitscheck U. J. Cell Biol. 2008; 183:77–86. [PubMed: 18824568]
50. Grunwald D, Singer RH. Nature. 2010; 467:604–607. [PubMed: 20844488]
51. Kahms M, Lehrich P, Sanetra JN, Peters R. Traffic. 2009; 10:1228–1242. [PubMed: 19548985]
52. Kubitscheck U, Grünwald D, Hoekstra A, Rohleder D, Kues T, Siebrasse JP, Peters R. J. Cell Biol. 2005; 168:233–243. [PubMed: 15657394]
53. Lowe AR, Siegel JJ, Kalab P, Siu M, Weis K, Liphardt JT. Nature. 2010; 467:600–603. [PubMed: 20811366]
54. Yang W, Gelles J, Musser SM. Proc. Natl. Acad. Sci. U. S. A. 2004; 101:12887–12892. [PubMed: 15306682]
55. Yang W, Musser SM. J. Cell Biol. 2006; 174:951–961. [PubMed: 16982803]
56. Sun C, Yang W, Tu LC, Musser SM. Proc. Natl. Acad. Sci. U. S. A. 2008; 105:8613–8618. [PubMed: 18562297]
57. Abu-Arish A, Kalab P, Ng-Kamstra J, Weis K, Fradin C. Biophys. J. 2009; 97:2164–2178. [PubMed: 19843449]
58. Ma J, Yang W. Proc. Natl. Acad. Sci. U. S. A. 2010; 107:7305–7310. [PubMed: 20368455]
59. Alber F, Dokudovskaya S, Veenhoff LM, Zhang W, Kipper J, Devos D, Suprapto A, Karni-Schmidt O, Williams R, Chait BT, Rout MP, Sali A. Nature. 2007; 450:683–694. [PubMed: 18046405]
60. Devos D, Dokudovskaya S, Williams R, Alber F, Eswar N, Chait BT, Rout MP, Sali A. Proc. Natl. Acad. Sci. U. S. A. 2006; 103:2172–2177. [PubMed: 16461911]
61. Schwartz TU. Curr. Opin. Struct. Biol. 2005; 15:221–226. [PubMed: 15837182]
62. Stoffler D, Fahrenkrog B, Aebi U. Curr. Opin. Cell Biol. 1999; 11:391–401. [PubMed: 10395558]
63. Paulillo SM, Phillips EM, Köser J, Sauder U, Ullman KS, Powers MA, Fahrenkrog B. J. Mol. Biol. 2005; 351:784–798. [PubMed: 16045929]
64. Lim RYH, Huang N-P, Köser J, Deng J, Lau KHA, Schwarz-Herion K, Fahrenkrog B, Aebi U. Proc. Natl. Acad. Sci. U. S. A. 2006; 103:9512–9517. [PubMed: 16769882]

NIH-PA Author Manuscript NIH-PA Author Manuscript NIH-PA Author Manuscript

65. Wälde S, Kehlenbach RH. Trends Cell Biol. 2010; 20:461, 469. [PubMed: 20627572]
66. Frey S, Görlich D. Cell. 2007; 130:512–523. [PubMed: 17693259]
67. Frey S, Gorlich D. EMBO J. 2009; 28:2554–2567. [PubMed: 19680227]
68. Frey S, Richter RP, Gorlich D. Science. 2006; 314:815–817. [PubMed: 17082456]
69. Patel SS, Belmont BJ, Sante JM, Rexach MF. Cell. 2007; 129:83–96. [PubMed: 17418788]
70. Yamada J. Mol. Cell. Proteomics. 2010; 9:2205–2224. [PubMed: 20368288]
71. Hess HF, Betzig E, Harris TD, Pfeiffer LN, West KW. Science. 1994; 264:1740–1745. [PubMed: 17839907]
72. Betzig E. Opt. Lett. 1995; 20:237–239. [PubMed: 19859146]
73. Patterson GH, Lippincott-Schwartz J. Science. 2002; 297:1873–1877. [PubMed: 12228718]
74. Thompson RE, Larson DR, Webb WW. Biophys. J. 2002; 82:2775–2783. [PubMed: 11964263]
75. Yildiz A, Forkey JN, McKinney SA, Ha T, Goldman YE, Selvin PR. Science. 2003; 300:2061–2065. [PubMed: 12791999]
76. Yildiz A, Park H, Safer D, Yang Z, Chen LQ, Selvin PR, Sweeney HL. J. Biol. Chem. 2004; 279:37223–37226. [PubMed: 15254036]
77. Fernandez-Suarez M, Ting AY. Nat. Rev. Mol. Cell Biol. 2008; 9:929–943. [PubMed: 19002208]
78. Lippincott-Schwartz J, Patterson GH. Trends Cell Biol. 2009; 19:555–565. [PubMed: 19836954]
79. Yildiz A, Tomishige M, Vale RD, Selvin PR. Science. 2004; 303:676–678. [PubMed: 14684828]
80. Zhuang X. Annu. Rev. Biophys. Biomol. Struct. 2005; 34:399–414. [PubMed: 15869396]
81. Cardarelli F, Gratton E. PLoS One. 2010; 5:e10475. [PubMed: 20454622]
82. Gustafsson MGL. Proc. Natl. Acad. Sci. U. S. A. 2005; 102:13081–13086. [PubMed: 16141335]
83. Yang W, Musser SM. Methods. 2006; 39:316–328. [PubMed: 16879979]
84. Hell SW, Kroug M. Appl. Phys. B: Lasers Opt. 1995; 60:495–497.
85. Rust MJ, Bates M, Zhuang X. Nat. Methods. 2006; 3:793–796. [PubMed: 16896339]
86. Betzig E, Patterson GH, Sougrat R, Lindwasser OW, Olenych S, Bonifacino JS, Davidson MW, Lippincott-Schwartz J, Hess HF. Science. 2006; 313:1642–1645. [PubMed: 16902090]
87. Hess ST, Girirajan TPK, Mason MD. Biophys. J. 2006; 91:4258–4272. [PubMed: 16980368]
88. Huang B, Bates M, Zhuang X. Annu. Rev. Biochem. 2009; 78:993–1016. [PubMed: 19489737]
89. Patterson G, Davidson M, Manley S, Lippincott-Schwartz J. Annu. Rev. Phys. Chem. 2010; 61:345–367. [PubMed: 20055680]
90. Huang B, Wang W, Bates M, Zhuang X. Science. 2008; 319:810–813. [PubMed: 18174397]
91. Ma J, Goryaynov A, Yang W. unpublished data. 2011
92. Grote G, Kubitscheck U, Reichelt R, Peters R. J. Cell Sci. 1995; 108:2963–2972. [PubMed: 8537436]
93. Stevens K, Swift H. J. Cell Biol. 1966; 31:55–77. [PubMed: 5971975]
94. Kopito A, Elbaum M. Proc. Natl. Acad. Sci. U. S. A. 2007; 104:12743–12748. [PubMed: 17646647]
95. Kampmann H, Atkinson CE, Mattheyses A, Simon SM. Nat. Struct. Mol. Biol. 2011; 18:643–649. [PubMed: 21499242]
96. Mattheyses AL, Kampmann M, Atkinson CE, Simon SM. Biophys. J. 2010; 99:1706–1717. [PubMed: 20858414]
97. Mohr J, Frey S, Fischer T, Guttler T, Gorlich D. EMBO J. 2009; 28:2541–2553. [PubMed: 19680228]
98. Fiserova D, Richards S, Wente S, Goldberg M. J. Cell Sci. 2010; 123:2773–2780. [PubMed: 20647373]
99. Shao L, Berith I, Satoru U, Agard AD, Sedat J, Gustafsson M. Biophys. J. 2008; 94:4971–4983. [PubMed: 18326649]
100. Schermelleh L, Carlton P, Haase S, Shao L, Winoto L, Kner P, Burke B, Cristina Cardoso M, Agard DA, Gustafsson M, Leonhardt H, Sedat J. Science. 2008; 320:1332–1336. [PubMed: 18535242]

NIH-PA Author Manuscript

NIH-PA Author Manuscript

NIH-PA Author Manuscript

101. Sung E, Sivaramakrishnan S, Dunn A, Spudich J. Methods Enzymol. 2010; 475:321–375. [PubMed: 20627164]

102. Mortensen K, Churchman L, Spudich J, Flyvbjerg H. Nat. Methods. 2010; 75:377–381. [PubMed: 20364147]

103. Siebrasse L, Peters R. EMBO Rep. 2002; 3:887–892. [PubMed: 12189172]

104. Tokunaga M, Imamoto N, Sakata-Sogawa K. Nat. Methods. 2008; 5:159–162. [PubMed: 18176568]

105. Hüve J, Wesselmann R, Kahms M, Peters R. Biophys. J. 2008; 95:877–885. [PubMed: 18375513]

NIH-PA Author Manuscript

NIH-PA Author Manuscript

NIH-PA Author Manuscript

Insight, innovation, integration

Nucleocytoplasmic transport provides an important focal nucleocytoplasmic transport, which could not be measured point for the relay of essential materials and information by conventional ensemble average methods. In this review, between the cytoplasm and the nucleus of eukaryotic cells. A we integrated data on the single-molecule characterization of critical question is how functional transport is maintained or, nucleocytoplasmic transport. In particular, we highlighted a through dysfunction, compromised. Using non-invasive imarecent advance from one-dimensional to three-dimensional ging of single bio-molecules in cells with a sub-light-diffraction characterization of transport through nuclear pore complexes spatial resolution, single-molecule fluorescence microscopy and presented a comprehensive understanding of the transport has been used to measure important kinetic values for mechanism obtained by this new technical development.

NIH-PA Author Manuscript

NIH-PA Author Manuscript

NIH-PA Author Manuscript

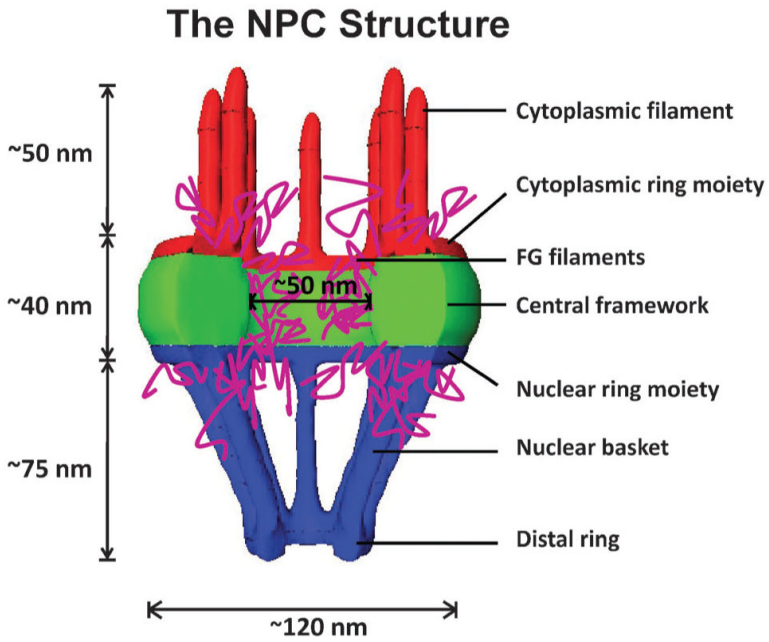

Fig. 1.

Schematic view of the nuclear pore complex. The NPC is composed of an octagonal central framework (green) that is ~40 nm in length and ~50 nm or ~120 nm in internal or external diameter. A cytoplasmic ring moiety with cytoplasmic filaments (red) of ~50 nm in total length is attached to the central framework on the cytoplasmic side of the NPC. The nuclear ring moiety and distal ring form a nuclear basket that is ~75 nm in length (blue), which is connected to the central framework on the nuclear side of the NPC. FG-filaments (purple) occlude the central channel of the NPC.

NIH-PA Author Manuscript

NIH-PA Author Manuscript

NIH-PA Author Manuscript

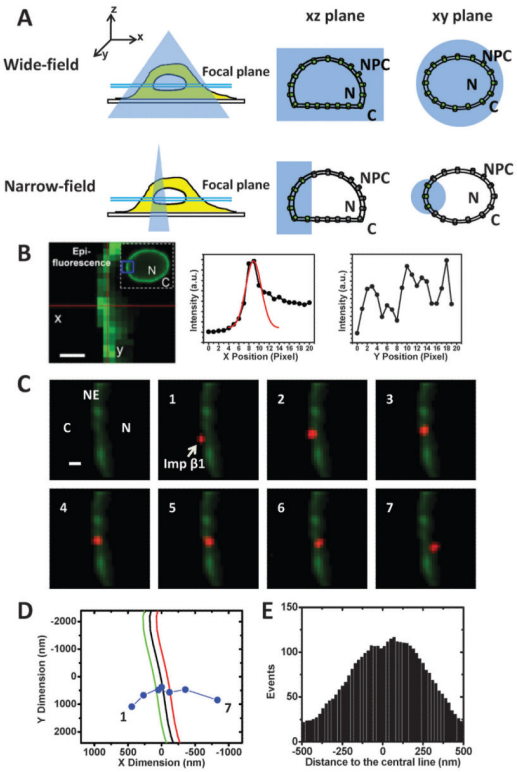

Fig. 2.

Single-molecule characterization of nucleocytoplasmic transport by wide-field and narrow-field epifluorescence microscopy. (A) In wide-field epifluorescence microscopy, an expanded, slightly diverged light excitation beam (blue shadow) overfills the back aperture of the objective and is focused into a diffraction-limited spot above the focal plane (between the two cyan lines) of the objective. A large excitation volume in the cell sample illuminates all GFP-NPCs (green) embedded in the NE in both the *xy* and *xz* planes. By contrast, a much narrower illumination volume in the sample is formed in narrow-field microscopy after the excitation light beam is confined by a pinhole in its path. As a result, only a few GFP-NPCs (green) inside the illumination volume are excited, and the other GFP-NPCs (grey) outside the volume remain non-fluorescent. N, the nucleus. C, the cytoplasm. (B) The fluorescent images of the NE at the equatorial plane of the HeLa cell nucleus. The heavily overlapped green fluorescence of the GFP-NPCs indicates the position of the NE in wide-field (inset) or narrow-field microcopy (the partial NE enclosed in the blue box of the inserted image). Scale bar: 1 μm. The line-scanned pixel intensities of these overlapped GFP-NPCs can be roughly fitted by a Gaussian function for each row in the *x* dimension but not in the *y* dimension. The peak positions of each Gaussian fit in the *x* dimension for a particular set of pixel intensities are subsequently fit with a second-degree polynomial, yielding the location of the middle plane of the NE within the excited area as shown in (D). (C) A typical import event of Imp β1 across the fluorescent NE. Consecutive video frames (1 ms per frame) show that an Alexa Fluor 647-labeled Imp β1 molecule (red dot) starts from the cytoplasm (C), interacts with the NE (green), escapes from the NE and enters the nucleus (N). Scale bar: 2 μm. (D) Trajectories (blue dots) of the interaction event shown in (C) from frames 1 to 7. The black curve is the experimentally determined position of the middle plane of the NE. The green and red curves are for reference at +100 nm and 100 nm from the middle plane of the NE, respectively. (E) 1D spatial distribution of single transiting molecules in the direction perpendicular to ±the tangent of the middle plane of the NE. Based on hundreds of single-molecule trajectories of transport events as shown in (D), a

histogram of the relative distances between the single-molecule spatial locations and the middle plane of the NE can be obtained.

NIH-PA Author Manuscript

NIH-PA Author Manuscript

NIH-PA Author Manuscript

NIH-PA Author Manuscript

NIH-PA Author Manuscript

NIH-PA Author Manuscript

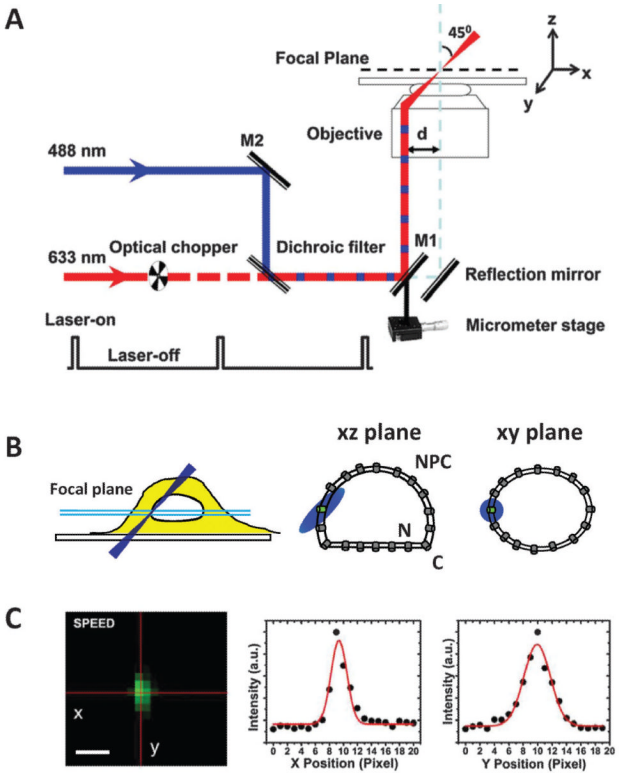

Fig. 3.

Setup for SPEED microscopy. (A) Diagram of the single-point edge excitation in SPEED microscopy. Equivalent to the illumination pattern of a 488 nm laser, the 633 nm laser is shifted about 237 μm from the center of the objective (d) by a micrometre stage to generate an inclined illumination volume at a 451 angle to the perpendicular direction. An optical chopper on the path of the 633 nm laser beam provides an on-off laser mode with a shorter laser-on time than the laser-off time. The longer laser-off time is sufficient for the transiting molecules in the NPC to escape from the illumination volume and for fresh cargo molecules with intact fluorescence to diffuse from the cytoplasm or the nucleus into the NPC. To ensure the imaging of complete transport events through the NPC, the photobleaching time of the single fluorescent molecules is longer than their nuclear transport time. (B) Diagram for the capture of a single GFP-NPC in both the *xz* and *xy* planes in a cell by SPEED microscopy. The incident 488 nm laser beam is shifted about 237 μm off the center of the objective to form an inclined illumination volume. The main goal of this adjustment is to reduce the illumination volume in the *z* direction and eventually illuminate only a single NPC in the three *xyz* dimensions. N, the nucleus. C, the cytoplasm. (C) A well-isolated fluorescent spot of a single GFP-NPC captured by SPEED microscopy. A 2D elliptical Gaussian function is used to fit the spot, and the centroid of the GFP-NPC is then determined with an approximately 1 nm localization accuracy. Scale bar: 1 μm.

NIH-PA Author Manuscript

NIH-PA Author Manuscript

NIH-PA Author Manuscript

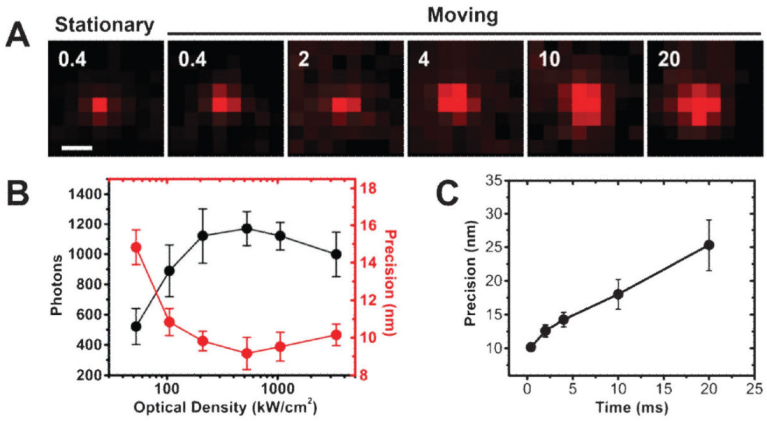

Fig. 4.

Localization precisions for stationary and moving Alexa Fluor 647-labeled Imp β1 molecules. (A) The fluorescent spots from single Imp β1 molecules adsorbed to the surface of a coverslip or moving in a solution mimicking that found inside the NPC (an estimated viscosity about 65 cp[55]) were measured with various detection times. The viscosity of the transport buffer was increased to around 65 cp by the addition of 81% glycerol and 1.5% PVP. β1 molecules were then tracked in the solution. Numbers denote time (ms). Scale bar: 500 nm. (B) The collected photons and localization precisions of single stationary Imp β1 molecules depend on the average optical density of the illumination volume. (C) The localization precisions of single moving Imp β1 molecules strongly depend on the detection time. As shown, with a 10 ms detection time, the localization precision was two-fold worse than that obtained with a detection time of 400 μs. Around 200 single molecules were collected for each point in (B) and (C).

NIH-PA Author Manuscript

NIH-PA Author Manuscript

NIH-PA Author Manuscript

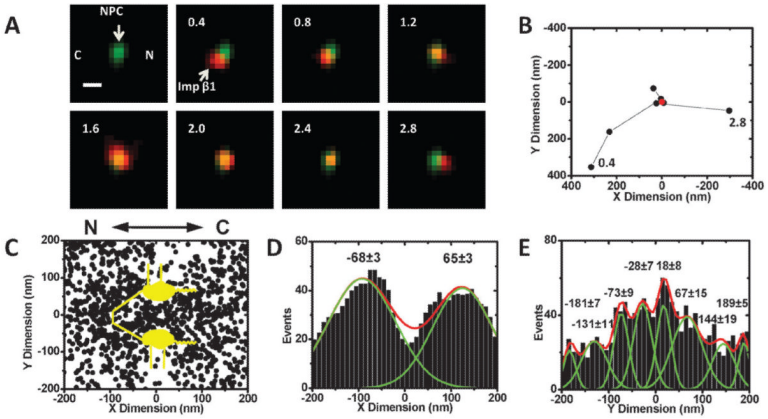

Fig. 5.

Imaging and tracking of single molecules in a single GFP-NPC by SPEED microscopy. (A-B) A typical single-molecule import event and its trajectories in a single native NPC captured by SPEED microscopy. A single Imp β1 molecule (red spot) started from the cytoplasm (C), interacted with the only illuminated GFP-NPC (green spot), and entered the nucleus (N). A series of consecutive video frames is shown, and the numbers denote time in milliseconds. Based on the single-molecule trajectories (black dots), the dimension and the centroid (a red dot in B) of the NPC, the Imp β1 molecule interacted with the NPC for 1.2 ms to 2.4 ms. N, the nucleoplasmic side of the NPC; C, the cytoplasmic side of the NPC. Scale bar: 1 μm. (C) Superimposed plots of thousands of Imp β1 single-molecule trajectories in single NPCs. Molecular spatial locations within an area of 400 × 400 nm around the centroid of the NPC are shown and further overlaid with a diagram of the NPC architecture (yellow). N, the nucleoplasmic side of the NPC; C, the cytoplasmic side of the NPC. (D) A histogram of the Imp β1 spatial locations within the NPC in the *x* dimension. The histogram is fit well by a combination of two Gaussian functions. (E) A histogram of the Imp β1 spatial locations within the NPC in the *y* dimension. The histogram is fit by multiple Gaussian functions.

NIH-PA Author Manuscript

NIH-PA Author Manuscript

NIH-PA Author Manuscript

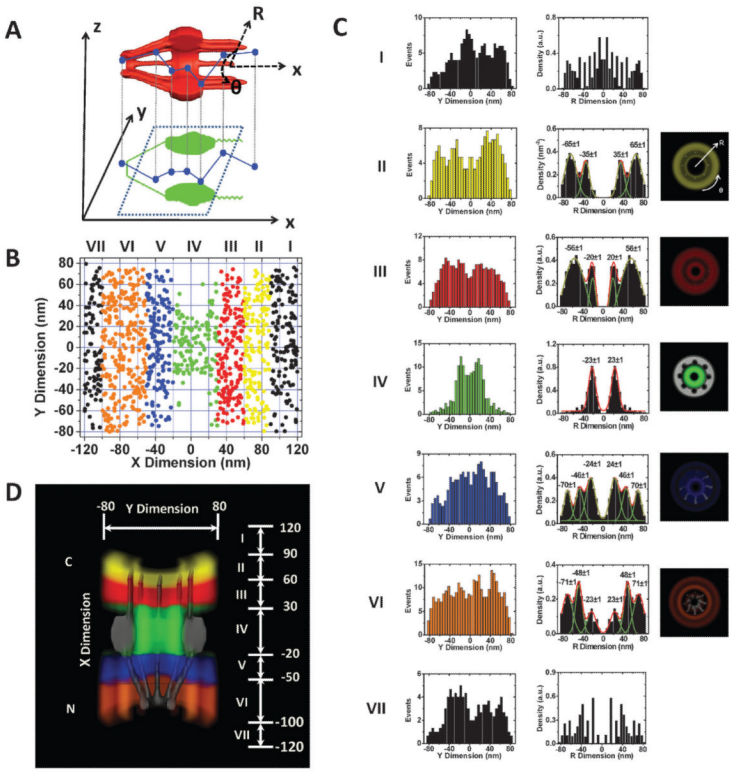

Fig. 6.

3D spatial density map of the interaction sites of Imp β1 in the NPCs. (A) The diagram demonstrates that the 2D spatial locations of Imp β1 obtained in the focal plane of the objective (the corresponding *xy* plane) are projections of the actual 3D spatial locations in the NPC. The 3D spatial locations can be described by a cylindrical coordinate system (*R, Θ, x*). Coordinate *x* represents the location along the NPC axis, whereas (*R, Θ*) refers to the positions at the cross-section of the NPC. (B) The 2D spatial locations of Imp β1 within the NPC are spatially divided into ranges I–VII and purposely plotted in seven different colors. The separated regions are based on the different clusters of the interaction sites between Imp β1 and the FG repeats in the NPC as shown in (C and D). (C) Histograms of the spatial densities of the Imp β1 molecules along the radii (R) at the cross-section of the NPC in ranges I–VII. The first column contains the histograms of the spatial locations of Imp β1 in ranges I–VII along the y dimension in (B), the second column contains the corresponding histograms in the R dimension after the deconvolution process (the major peaks are obtained by Gaussian fittings), and the third column is the cross-sectional image of each region. Because the Imp β1 spatial locations are randomly distributed outside the NPC, there is no interaction group in ranges I or VII. Bin size: 5 nm. (D) Cutaway view of the 3D spatial density map of Imp β1 superimposed on the NPC architecture (gray). Different colored regions illustrate different spatial configurations driven by the interactions between Imp β1 and the FG repeats in the NPC. The numbers in nanometres denote the distance from the centroid of the NPC.

NIH-PA Author Manuscript

NIH-PA Author Manuscript

NIH-PA Author Manuscript

Table 1

Selected examples of single-molecule fluorescence microscopy studies of nucleocytoplasmic transport (1D, 3D and N/A refer one dimension, three dimensions and not available, respectively)

Object of study	Technique	Localization of transiting molecules in the NE/NPC	Main observations/ conclusions	References
Nucleocytoplasmic transport rates of NTF2 and GFP in isolated nuclei and nuclear envelope.	Optical single transporter recording (OSTR)	N/A	NTF2 transport through the NPC about 30-times faster than the same-sized GFP.	103
Protein facilitated translocation through NPCs by using NLS-2xGFP in permeabilized cells.	Narrow-field epifluorescence	1D	Protein cargo complexes spend 9–10 ms interacting within NPC, moving rapidly in a random walk; the rate-limiting step is the substrate exit from the pore	54
Investigate the nuclear import of influenza genes, in the form of ribonucleoproteins (vRNPs), by imaging single vRNPs in living cells.	Wide-field epifluorescence	1D	The influenza M1 protein, a regulatory protein for the import process, downregulates the nuclear import of vRNPs by inhibiting the interactions between vRNPs and NPCs.	48
Transport receptors (NTF2 and transportin) and their cargo complexes transport through the NPC in permeabilized cells.	Wide-field epifluorescence	1D	NTF2 and transportin interact with the NPC by approximately 5.8 and 7.2 ms respectively. The times were reduced upon binding of cargo.	52
Transport times and efficiencies of passive and facilitated transport through the NPC depend on the concentration of Imp β1 in both permeabilized and live cells.	Narrow-field epifluorescence	1D	Imp β1 concentration in the nuclear pore can accelerate the transport rates for either passive diffusion of small dextran molecules or NLS-2xGFP/Imp α1/Imp β1 complex. The results were directly compared to the corresponding measurements in live cells.	55
Single-molecule fluorescence resonance energy transfer (FRET) was applied to determine the dissociating process of import cargo complexes in the NPCs of permeabilized cells.	Narrow-field epifluorescence	1D	The three hypotheses describing Importin α and cargo dissociating process and locations within NPCs, have been tested by measuring single molecule FRET rates between Importin a and cargo. The results indicated that their dissociation occurs at the nuclear basket where both CAS (a recycling cofactor for Importin α) and Nup50 have to present for effective dissociation.	56
Measurements of number of GFP-Importin β1 molecules bound to a single NPC of permeabilized cells.	Highly inclined and laminated optical sheet (HILO)	N/A	A dissociation constant of about 70 nM and a maximum bound number of approximately 110 Importin β1 molecules per NPC.	104
Transport times for more transport receptors were measured in live cells.	Wide-field epifluorescence	1D	The transport times fall in the range of 5–8 ms for Imp α, Imp β1 and transportin	49
Binding site distribution of NTF2 and Imp β1 in the NPC in permeabilized cells.	Wide-field epifluorescence	1D	Two major binding sites for NTF2 in the NPC located at 30 and 10 nm from the middle	51

NIH-PA Author Manuscript

NIH-PA Author Manuscript

NIH-PA Author Manuscript

Object of study	Technique	Localization of transiting molecules in the NE/NPC	Main observations/ conclusions	References
			plane of NE biased to the cytoplasmic side. The 10 nm location is also a major bidning site for Imp β1.	
Topographic features of single NPC	4-PI microscopy	N/A	By immune-labeled Nups on either side and GFP-fused central Nups, the distance between the NPC center and either side of NPC was determined by 4PI microscopy.	105
The distribution and dynamics of an enhanced yellow fluorescent protein (EYFP)-Ran in live cells.	Fluorescence recovery after photobleaching (FRAP), FCS and Raster-image correlation spectroscopy	1D	Only a fraction of the Ran concentrated at the NE transits into nucleus.	57
Export of mRNA through the NPC in live cells.	Wide-field epifluorescence	1D	The measured kinetics of mRNA transport in mammalian cells present a three-step model consisting of docking (80 ms), transport (5–20 ms) and release (80 ms), totaling 180 ms.	50
Single protein-functionalized quantum dots were used as cargos to study nucleocytoplasmic transport in permeabilized cells.	Wide-field epifluorescence	1D	Cargo movement in the central channel is subdiffusive and cargos that can bind more transport receptors diffuse more freely. The overall selectivity of the NPC seems to arise from the cumulative action of multiple reversible substeps and a final irreversible exit step.	53
Capture transient interactions between cargo-free or cargo-bound Imp β1 and single NPCs with a high spatiotemporal resolution. The real-time 3D density maps of transient interaction sites in the native NPCs were provided for the first time.	SPEED microscopy	3D	SPEED microscopy enables snapshots of transient interactions between transport receptors and the FG-barrier in native NPCs with a spatiotemporal resolution of 9 nm and 400 μs. By a deconvolution algorithm, 3D density maps of cargo-free and cargo-bound Imp β1 were obtained. The new methodologies provide novel insight in nucleocytoplasmic transport mechanism.	58